Tomas Bata University in Zlín
Library

Mechanical strain and electric-field modulation of graphene transistors integrated on MEMS cantilevers

Citation

GABLECH, Imrich, Jan BRODSKÝ, Petr VYROUBAL, Jakub PIASTEK, Miroslav BARTOŠÍK, and Jan PEKÁREK. Mechanical strain and electric-field modulation of graphene transistors integrated on MEMS cantilevers. *Journal of Materials Science* [online]. vol. 57, Springer, 2022, p. 1923 - 1935 [cit. 2023-02-06]. ISSN 0022-2461. Available at https://link.springer.com/article/10.1007%2Fs10853-021-06846-6

DOI

https://doi.org/10.1007/s10853-021-06846-6

Permanent link

https://publikace.k.utb.cz/handle/10563/1010781

This document is the Accepted Manuscipt version of the article that can be shared via institutional repository.

TBU Publications
Repository of TBU Publications
publikace.k.utb.cz

Mechanical strain and electric-field modulation of graphene transistors integrated on MEMS cantilevers

Imrich Gablech, Jan Brodský, Petr Vyroubal, Jakub Piastek, Miroslav Bartošík and Jan Pekárek**

Dr. I. Gablech, J. Brodský, Dr. J. Pekárek, J. Piastek, Dr. M. Bartošík
Central European Institute of Technology, Brno University of Technology,
Purkyňova 123, 612 00 Brno, Czech Republic
E-mail: imrich.gablech@ceitec.vutbr.cz, pekarek@vutbr.cz

Dr. P. Vyroubal
Department of Electrical and Electronic Technology, Faculty of Electrical Engineering and Communication, Brno University of Technology, Technická 3058/10, 616 00 Brno, Czech Republic

Keywords: graphene FET, MEMS, cantilever, strain, stress

This work proposes a structure which allows characterization of graphene monolayers under combined electric field and mechanical strain modulation. Our approach is based on a cantilever integrated into a two-dimensional graphene-based field effect transistor (FET). This allows us to change graphene properties either separately or together via two methods. The first way involves electric field induced by the gate. The second is induction of mechanical strain caused by external force pushing the cantilever up or down. We fabricated devices using silicon-on-insulator wafer with practically zero value of residual stress and a high-quality dielectric layer which allowed us to precisely characterize structures using both mentioned stimuli. We used the electric field/strain interplay to control resistivity and position of the charge neutrality point often described as the Dirac point of graphene. Furthermore, values of mechanical stress can be obtained during the preparation of thin films, which enables the cantilever to bend after the structure is released. Our device demonstrates a novel method of tuning the physical properties of graphene in silicon and/or complementary metal-oxide-semiconductor technology, and is thus promising for tunable physical or chemical sensors.

1. Introduction

Graphene as a unique material is used for physical and chemical sensing. Several types of gas and vapor nanosensors employing graphene were reported [1,2]. To this end, graphene is most often deployed in resistive sensors [3], field effect transistors (FET) [4], surface acoustic wave (SAW) sensors [5], quartz crystal microbalance (QCM) sensors [6], microelectromechanical systems (MEMS) or nanoelectromechanical systems (NEMS), gravimetric sensors [7], MEMS or NEMS infrared (IR) detectors [8], and semiconductor modified hybrid sensors [9].

A single layer of carbon atoms in the sp^2 hybridization arranged in a hexagonal (honeycomb) lattice called graphene was first calculated using the tight-binding method by Wallace as a model for graphite in 1946 [10] and prepared by Geim and Novoselov in 2004 [11]. It has been an extensively studied material with numerous interesting thermal, mechanical, electrical, and optical properties [12-14]. As a monatomic layer, it exhibits a high mechanical flexibility and ambipolar electrical charge transport [14].

Furthermore, its electronic properties, such as electrical charge mobility, can be greatly influenced by induced strain. Stretching graphene results in changes of the bond length between neighboring atoms in its lattice. This has a strong effect on the electronic transport properties of graphene. This influence is not yet completely understood, and it is an avenue of many possibilities worth exploring [15]. Measurement of graphene properties as a function of the controlled induced strain can be used for determination of the strain's influence on the graphene's electrical properties. Charge carrier mobility is an essential part of any electronic device, and altering it means that we can tailor the device parameters. The electrical conductivity and mechanical strength of graphene in the in-plane direction are much higher than those in the out-plane direction. Thus, the anisotropy in the physical properties of graphene can be obtained by its orientation [16].

Uniaxial and biaxial strain on graphene has been studied using a variety of methods, schematized in Figure 1. Uniaxial strain was induced by bending graphene on a deformable substrate (Figure 1A) and subsequently characterized using Raman spectroscopy to probe its phonon modes [17,18]. The uniaxial strain moves the relative positions of the Dirac points and has a significant influence on the intervalley double-resonance processes (D and 2D peaks).

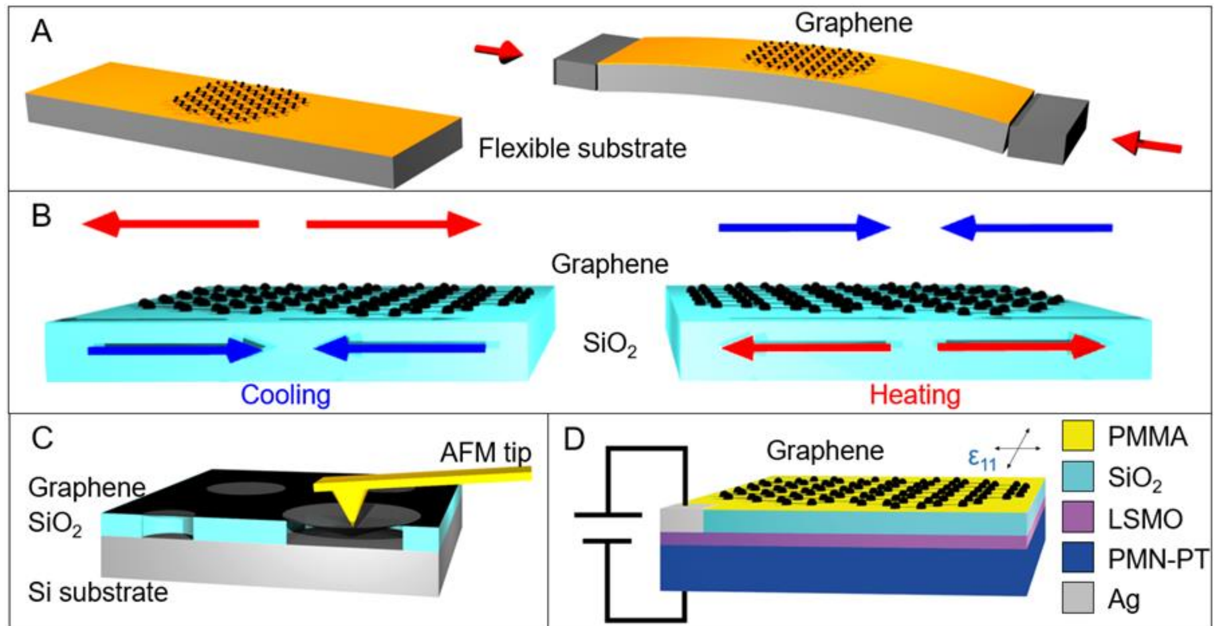

Figure 1. Schematic of engineering strain on graphene: A) uniaxial straining on a flexible substrate, B) thermal expansion and contraction of graphene on thermally heated or cooled SiO_2 substrate, C) suspended graphene membrane nanoindentation, D) the electromechanical device for inducing in-plane biaxial strain to the graphene.

Biaxial strain is more suited to studying the strain effects on the double-resonance processes since it mimics the realistic experimental conditions where the graphene is supported by a planar substrate. Biaxial strain in graphene can be intentionally induced and controlled by three commonly used methods:

1. The graphene is placed on a material with a different thermal coefficient of expansion, and is subjected to temperature changes, causing the graphene to stretch (Figure 1B) [19].

2. The graphene is clamped across a hole in a substrate, and it is mechanically stretched by pushing the graphene into the hole using an atomic force microscopy tip (Figure 1C) [20] or electrostatically [21].

3. The graphene can be transferred onto a piezoelectric substrate, which is controllably shrunk or elongated by applying a bias voltage. It results in the graphene having a uniform biaxial strain (Figure 1D) [22].

Graphene is known as an excellent material capable of sustaining reversible elastic tensile strain as large as 25 % [23]. This feature can be used to control graphene's electrical properties either statically or dynamically by integrating them with cantilevers leading to the novel applications of graphene [23]. These cantilevers based on MEMS or NEMS can be made of various materials. They can significantly impact the final structural properties, such as residual stress, stiffness, strain, resonance frequency, and quality factor. The structure should be fabricated by planar technology as it is a MEMS/NEMS process. Planar process compatibility offers monolithic integration of a sensing part with readout electronic circuits [24]. Biocompatibility further increases its attractiveness as it can be used in healthcare [25] to measure and detect cells, enzymes, amino acids, deoxyribonucleic acid, ribonucleic acid, etc. [26]. MEMS-based cantilever sensors have been demonstrated as feasible alternative solutions to the conventional assaying tools due to advantages such as compactness, lower detection limits, better sensitivity, cost-effectiveness, and real-time operation [27].

In this work, we studied the graphene monolayer through the simple complementary metal-oxide semiconductor (CMOS)-compatible MEMS cantilever with planar 2D-FET structure. We electrically characterized graphene on the cantilever under different conditions such as an applied electric field and uniaxial strain. These characterizations are supported by ANSYS® Workbench mechanical analysis. We confirmed the quality of the prepared graphene by measuring its Raman spectroscopy and showing the significant peaks. Here, we demonstrate the technological processing and the utilization of the proposed structure for 2D-material strain engineering.

2. Experimental details

This chapter focuses on experimental details describing the most important aspects for device functionality and its fabrication to achieve graphene properties modulation in Si-based technology. Figure XX represents the idea of device, process flow and fundamental characterization methods used for behavior determination based on electrical and mechanical stimuli.

2.1. Device Design

Our goal was to fabricate a single-clamped beam (cantilever) with 2D-FET structure for the electrical measurement of graphene subjected to mechanical strain in static mode. Here, we discuss a few important layout parameters related to the cantilever. We designed a device with (6 × 6) mm^2 dimensions containing the array of 64 cantilevers (**Figure** 2). The width and length of the cantilevers were 60 µm and 100 µm, respectively. The dimensions of the cantilever were chosen and based on our fabrication experience to make this structure easily fabricated with no critical dimensions. The length was set according to maximum achievable displacement of the micromanipulator used for cantilever bending. These dimensions do not affect the bending profile of the cantilever as much as the (3.0 ± 0.5) µm thickness of Si, causing the high value of stiffness with the largest strain values on the fixed-end of cantilever. The cantilevers contain two electrodes for graphene connection placed at the clamped end of the cantilever. The gap between the electrodes determined the length of the graphene FET was set to 25 µm. Finally, the graphene width was set to 10 µm. The relatively large size of the cantilever allowed us to precisely place a micromanipulator tip for bending on the free end of the cantilever. The gate electrode is electrically contacted from the top side through the (100 × 100) $µm^2$ window in the top gate SiO_2 layer. We also employed van der Pauw structures allowing us to measure and evaluate sheet resistance of the metal layer. The dimension of all pads for probe contacts were (100 × 100) $µm^2$.

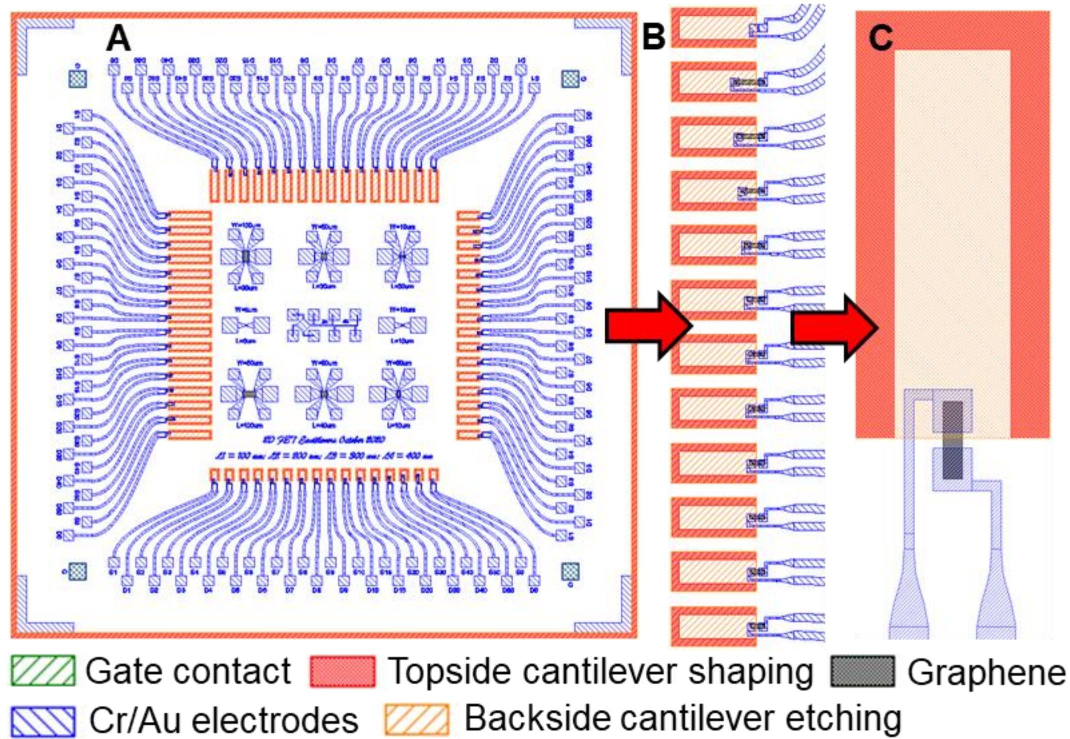

Figure 2. Layout of 2D-FET device with structures for graphene strain modulation: A) whole device with dimensions of (6 × 6) mm^2; B) cantilever array; C) electrodes connected to shaped graphene.

2.2. Fabrication

The fabrication of the device was done using five lithography steps (Figure 3), including graphene patterning. The chosen substrate was Silicon on Insulator (SOI) wafer with structural (handle) Si thickness of (500 ± 10) μm and diameter of (100.0 ± 0.5) mm, while the insulation (buried SiO_2) layer was (0.50 ± 0.25) μm thick. N-doped device Si (100) layer with thickness of (3.0 ± 0.5) μm was highly conductive with resistivity < 0.005 Ω·cm. As the first step, we grew ≈ 100 nm of SiO_2 on both sides of the substrate using the thermal oxidation process.

Next, we coated bottom resist AR-BR 5480 and positive photoresist (PR) AZ 5214 E enabling etching of SiO_2 window and lift-off process employing one lithography step to fabricate contacts to the gate electrode. The gate electrode was formed by the device Si layer of SOI wafer. SiO_2 was etched by $CHF_3/Ar/O_2$ plasma in a reactive ion etching (RIE) system.

Subsequently, we deposited ≈ 3 nm of Ti and ≈ 50 nm of Au and lift-off process was performed in 1-Methyl-2-pyrrolidone (NMP) solution at ≈ 80 °C rinsed in propan-2-ol (IPA) and finished with O_2 plasma cleaning (Figure 3B). In the second step, we coated the substrate with the same positive PR as before. Then, we used deep reactive ion etching (DRIE) of the device Si layer to shape the cantilevers from top side (Figure 3C). This process was followed by the same cleaning procedure as before.

In the next step, we transferred graphene via the wet-transfer method. The CVD-grown single-layer graphene on ≈ 100 mm of Cu foil (fabricated by Graphenea S.A., Spain) was coated with a double-layer of polymethyl methacrylate (PMMA), and the non-coated side of the Cu foil was cleansed with O_2 plasma. We dissolved the Cu layer through wet etching in an $FeNO_3$ solution. The floated PMMA/graphene stack layer was scooped out and displaced into a beaker filled with deionized (DI) water purified by the Millipore system to wash the solution residues out. Finally, the PMMA/graphene layer was transferred onto fabricated device and dried under a low flux of N_2. The transfer process was completed with the removal of the PMMA layer in an acetone bath overnight at ≈ 53 °C, followed by washing with IPA and DI water and drying with N_2. The CVD method is the most suitable for tasks in this framework due to the sufficient quality of graphene and the ability to cover a large area.

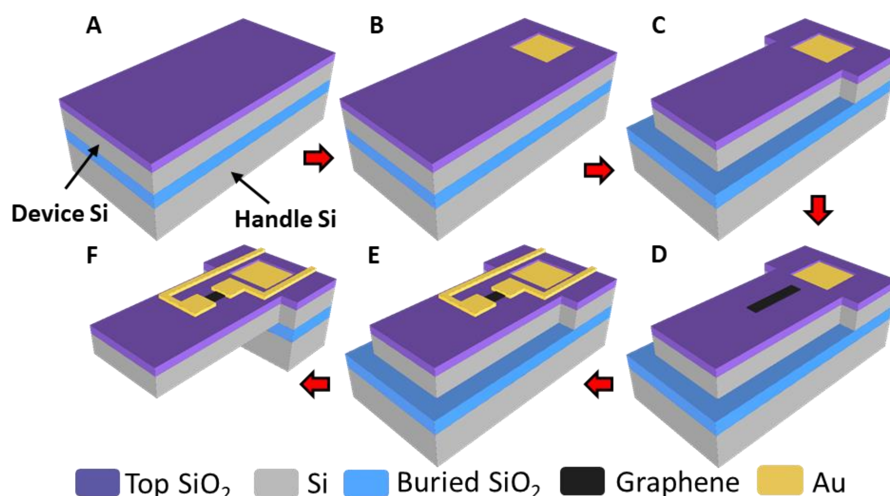

Figure 3. Fabrication flow of cantilever with 2D-FET structure for graphene strain engineering: A) substrate with deposited SiO_2 layer; B) gate contact after SiO_2 etching and

Ti/Au lift-off; C) shaping of the cantilever from topside; D) graphene shaping; E) Cr/Au electrode lift-off; F) releasing the cantilever from the bottom side.

The graphene was subsequently patterned (Figure 3D) using lithography with the PMMA AR-P 639.04 and AZ 5214 E PR. After the development, we used RIE, employing O_2 plasma to etch the PMMA and graphene, which took 300 s with power of ≈ 50 W at constant pressure of ≈ 0.25 Pa. Subsequently, we cleaned the wafer in acetone at ≈ 35 °C and dried it with N_2. The patterning was followed by the same lift-off process as before to create contact electrodes (Figure 3E) for graphene. In this step, we evaporated ≈ 3 nm of Cr and ≈ 100 nm of Au, followed by the same cleaning procedure as before excluding the O_2 cleaning step. The last lithography step was aimed at shaping the cantilever (Figure 3F) from the backside of the wafer using etching of SiO_2/handle Si/SiO_2 via DRIE. The wafer was split into single devices during the last etching step, meaning no dice cutting was necessary. The fabricated device is shown in Figure 4. The PR was removed in NMP solution and rinsed by IPA after these steps. After these steps, we mounted devices into a leadless carrier chip with 68 pads (LCC68) using epoxy paste EPOTEK H31-D and dried the whole device at ≈ 95 °C for 4 hours in the vacuum furnace at pressure of ≈ 5×10^{-4} Pa to ensure stable mechanical connection, which is sufficient for using the device in temperatures up to ≈ 200 °C. The last step of fabrication was wire-bonding using Au wire with a diameter of ≈ 25 μm, and the package with the device was placed into a socket on printed circuit board with SMA terminals.

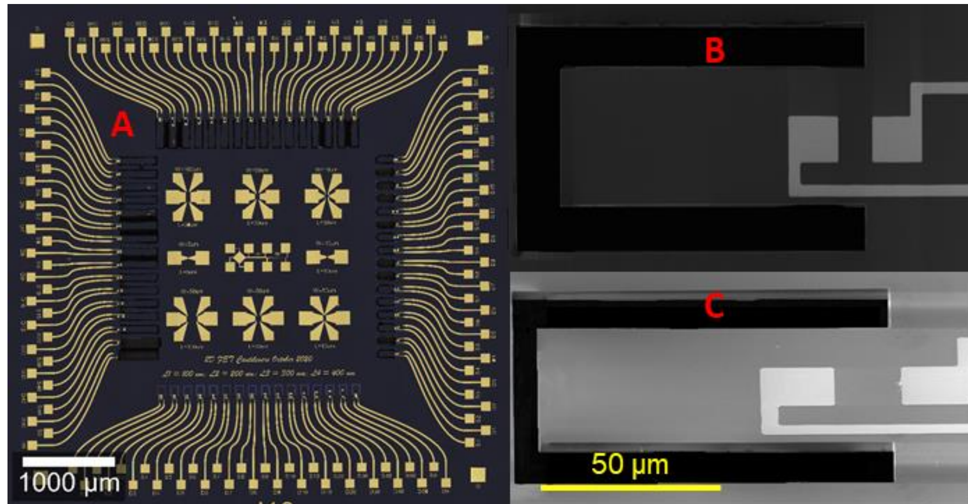

Figure 4. A) Optical image of fabricated chip; B) SEM image of cantilever from topside; C) SEM image of cantilever tilted by 55°.

2.3. Finite Element Analysis

We performed static structural analysis using ANSYS® Workbench to determine the value of stress and strain induced to the fixed end of the cantilever. A finite element method (FEM) was used for analysis of the single-clamped cantilever. The corresponding material properties were set for each part of the model.

We chose the following types of elements for mesh generation. We used quadratic element type SOLID186, which is higher order 3D 20-node solid element that exhibits quadratic displacement behavior. Additionally, the contacts between parts were bonded to each layer, which is due to the chip construction, so the layers could not slip separately onto each other. Thus, we used the CONTA174 element, representing behavior of the contact and the slide between 3D target surfaces and a deformable surface, and TARGE170, which represents the 3D target surfaces for the associated contact elements. We also used SHELL281, which is suitable for analyzing thin to moderately thick shell structures. This element has eight nodes with six degrees of freedom at each node. This element was used for thin graphene geometry because of structure thickness of ≈ 170 pm, with lower order thickness than the rest of the model, so it must be modeled as a thin-walled entity.

We set the steady-state numerical model with 15 sub-steps, defining the displacement in ranges from −70 μm to 70 μm with two boundary conditions (**Figure 5**). The left side of the cantilever, with the graphene, was set as fixed support, and the right side of the cantilever was attributed to displacement sweeping.

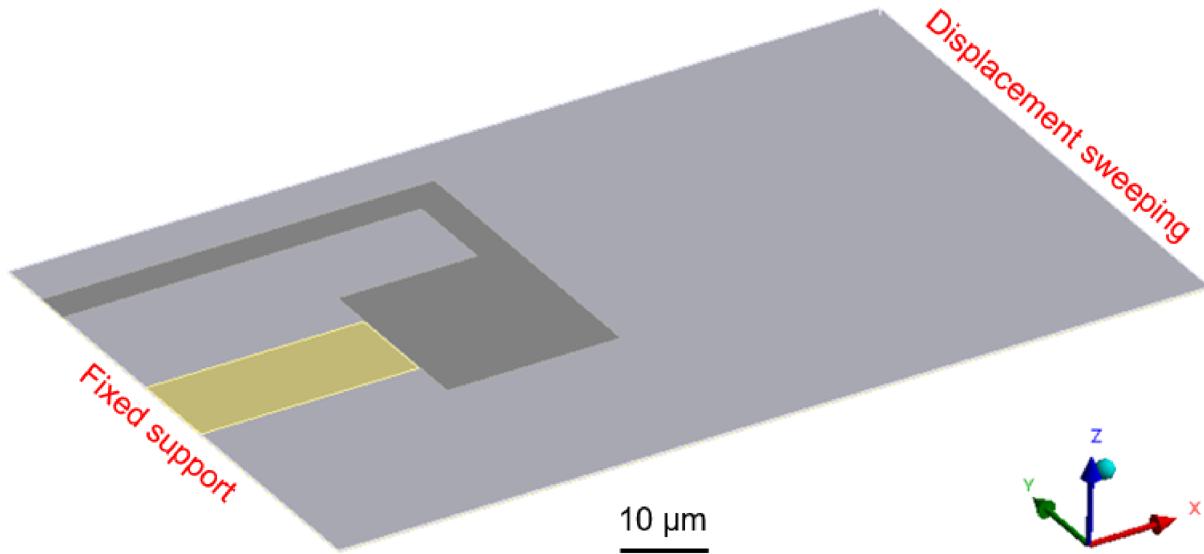

Figure 5. 3D model of structure for ANSYS® Workbench computation showing the boundary conditions.

2.4. Raman Spectra of Graphene

We measured the Raman spectra of graphene once the device was fabricated. We used the Confocal Raman imaging system Alpha 300R by WITEC, which employs a green laser with a wavelength of ≈ 532 nm and an optical microscope with objective magnification of 100× (numerical aperture of 0.9 and working distance of 0.31 mm). Grating with 600 grooves·mm^{-1} was used. Integration time was set to 2 s with number of accumulations set to 20 to suppress the distortion in obtained spectra.

2.5. Electrical Measurement

We measured the current between the source and drain electrodes (I_{DS}) by changing drain-source voltage (V_{DS}) at different gate-source voltages (V_{GS}). We also monitored the gate current (I_G) to inspect eventual current leak through the dielectric SiO_2 layer. The measurements were done in a N_2 atmosphere to avoid I_{DS} fluctuations due to unstable air humidity and for preventing other sorption phenomena on local graphene defects. We used a probe station MPS

150 (Cascade Microtech, USA) connected with the parameter analyzer 4200A SCS (Keithley instruments, USA). In case of the dependency of I_{DS} on mechanical strain induced by cantilever and V_{GS}, we used the micromanipulator with tip which was aimed perpendicularly to the end of the cantilever.

3. Results and discussion

3.1. Quality of Transferred Graphene

Since the chips with graphene were prepared, we wanted to check the number of graphene layers and their quality. Thus, we employed Raman spectroscopy to obtain significant graphene peaks in the Raman spectrum. We set the laser power to 5 mW, since it has been experimentally proven that higher power damages the graphene. Recorded Raman spectrum and maps are depicted in Figure 6.

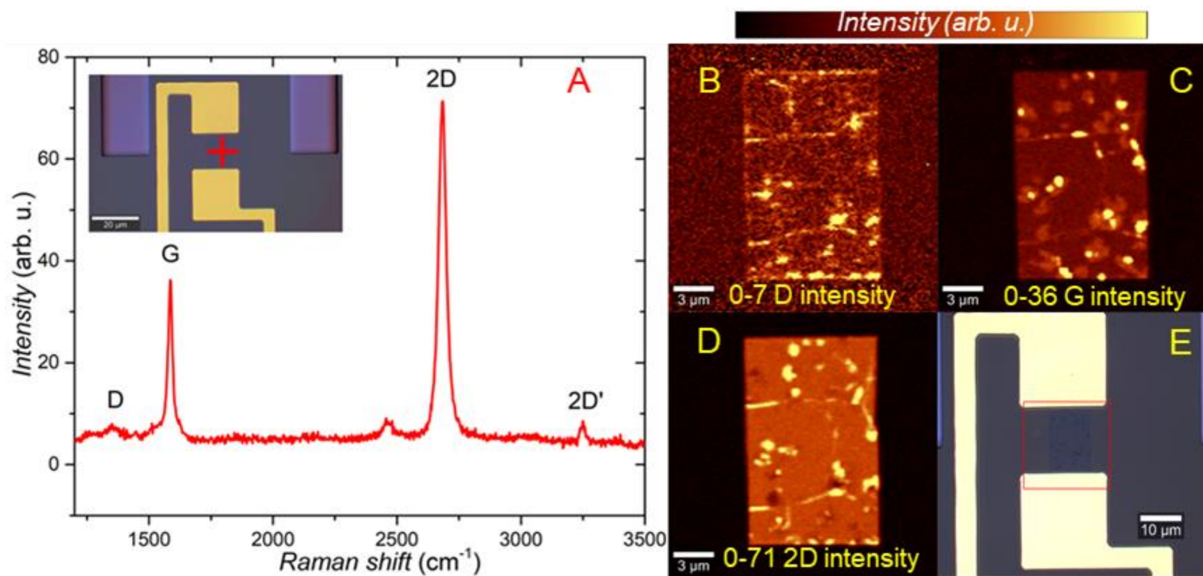

Figure 6. Raman spectra of graphene on structure after patterning: A) single spectra after patterning; Raman map of B) D peak, (C) G peak; (D) 2D peak; E) optical image of electrode with graphene.

The peak position of the G and 2D peaks was at ≈ 1592 cm^{-1} and ≈ 2677 cm^{-1}, respectively. Obtained Raman spectra show the high quality of the transferred graphene. The ratio of the G and 2D peaks (≈ 1:2) proves that the transferred graphene is single-layered [28]. The low intensity of the D peak shows very low presence of defects [29]. However, as seen in Figure 6B, the intensity of D peak is higher in specific locations, suggesting local abnormalities in graphene disorder, which is also visible in the optical image (Figure 6E). That being said, the quality of the patterned graphene area is still more than sufficient, since most of the area has very low D-peak intensity and the defects accumulate only in local spots. Such quality is enough

for intended application focused on stretching of the graphene and evaluation of the change in electrical properties.

3.2. Simulation of Strain and Stress

We applied mechanical force emulating the tip of the micromanipulator, causing strain through the bending of the free end of the cantilever. We did the simulation for the cantilever with a length of 100 µm with an etched hole underneath of ≈ 70 µm, which was experimentally determined by a contact profilometer. Thus, we simulated the influence of displacement on the free end of the cantilever along the z axis (d_z) with a range from −70 µm to +70 µm on the induced strain and stress (Figure 7).

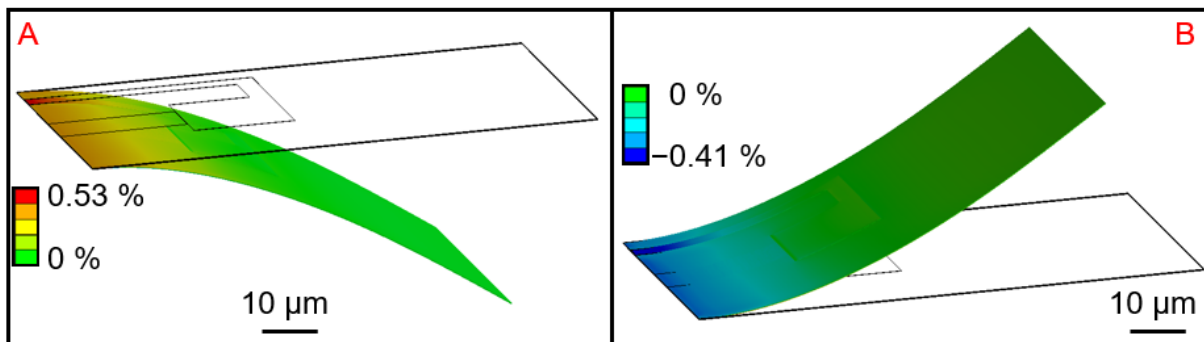

Figure 7. Obtained ε_{max} values from ANSYS® Workbench for the cantilever: A) bent down to −70 µm causing tensile strain to graphene; B) bent up to +70 µm along z-axis causing compressive strain to graphene.

Normal elastic strain (ε) and stress (σ) were evaluated on the model. The values of ε_{max} dependency on d_z were plotted in Figure 8A. From the σ/ε curve (Figure 8B), the highest value of ε_{max} and σ_{max} on the model was at maximal d_z of −70 µm and +70 µm at the fixed end of the cantilever. These values of ε_{max} and σ_{max} for the downward bent cantilever were ≈ 0.53% and ≈ 2.59 GPa, respectively. The maximal values for the bend in the opposite direction were ≈ −0.41% and ≈ −2.58 GPa, respectively. Such a value of σ_{max} can be achieved and further controlled by deposition parameters, which will allow the fabrication of device containing structures with pre-stressed layers and will cause the bending of structure upon releasing.

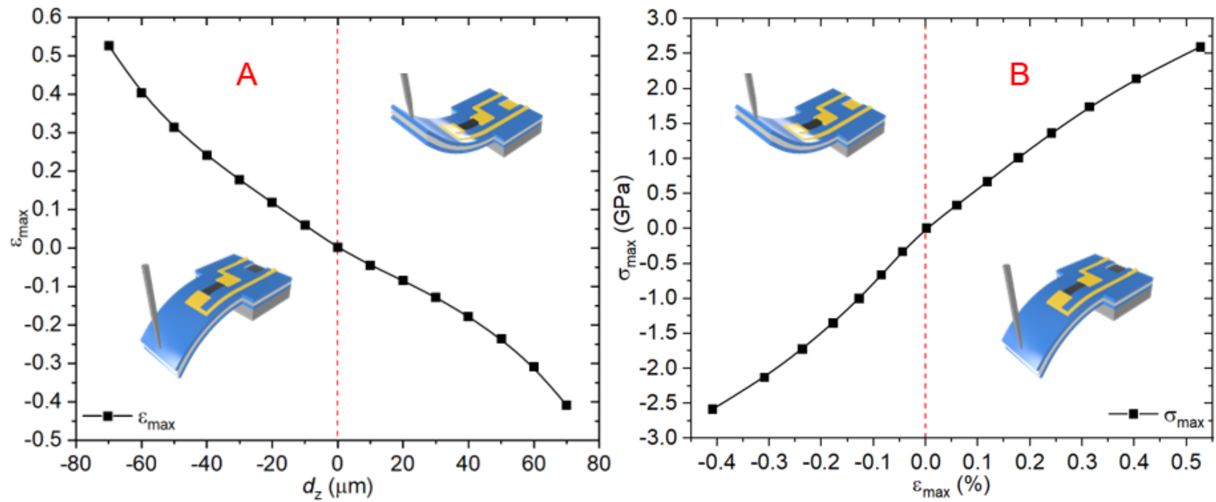

Figure 8. Obtained ε_{max} values from ANSYS® Workbench for the cantilever: A) bent down to −70 μm; B) bent up to +70 μm along z-axis.

3.3. Electrical Characterization of the 2D-FET Structure

We measured I_{DS} dependence on V_{DS} for different V_{GS} of 2D-FET graphene-based structures after the device was fabricated. Prior to electrical measurements, the sample was soaked in acetone for 24 hours and also annealed in vacuum furnace at ≈ 150 °C for 36 hours with low temperature ramp of ≈ 3 °C·min^{-1}. Dirac point voltage (V_{Dirac}) of pristine graphene should be at value of V_{GS} ≈ 0 V. However, when exposed to air, the graphene becomes p-doped [30,31] and the Dirac point moves towards higher values of V_{GS}. This is related to the adsorption of water from air humidity. The cleaning of graphene samples in acetone and annealing partly restores the original position of Dirac point. We wanted to prove the behavior of graphene employed as 2D-FET structure. We also measured the I_{DS} dependence on V_{GS} (transfer characteristics). The output characteristics were measured for V_{DS} in a range from −1 V to +1 V. Because of the excellent quality of the SiO_2 serving as the gate dielectric, we were able to sweep the V_{GS} in a range from −50 V to +50 V with 10 V step, without any significant leakage current (I_G), which was monitored during all experiments and was in the order of pA units. Throughout these measurements, we verified the functionality of 2D-FET structure with corresponding output characteristics that are shown in Figure 9. We observed normal behavior of gated p-doped graphene, showing a decrease in conductivity with V_{GS} near Dirac point of graphene.

The p-doping can be attributed to the residual water molecules [30] as a consequence of sample manipulation and measurement at atmospheric conditions.

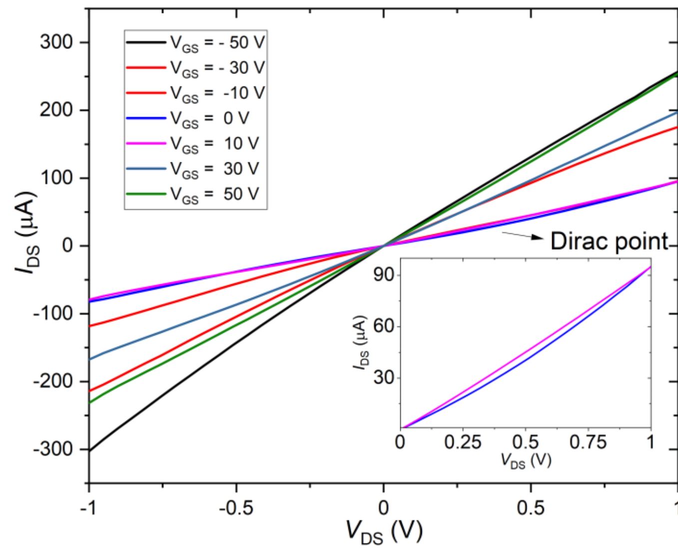

Figure 9. Output characteristics of graphene-based FET structure in range of V_{DS} from −1 V to 1 V for different V_{GS}. The detail of I_{DS} in dependence on V_{DS} for V_{DS} in the range from 0 V to 1 V is depicted in the inset.

3.4 Influence of the Cantilever Bending on I_{DS}

As the last step, we measured I_{DS} during the cantilever bending along the z-axis at constant V_{DS} = 1 V. We also changed the V_{GS} within the same range of previous measurements. The free end of the cantilever was firmly bent by the microtip fixed on sliding table with possible movement in the range from −70 μm to +70 μm along the z-axis. We observed a significant change of I_{DS} (Figure 10), which was dependent on the bending. For the first set of measurements, we used a bent probe with adhesive on the tip to bend the cantilever first in downwards direction and then in the upwards direction, hence, such measurement is not so accurate, but interesting prediction for next experiment.

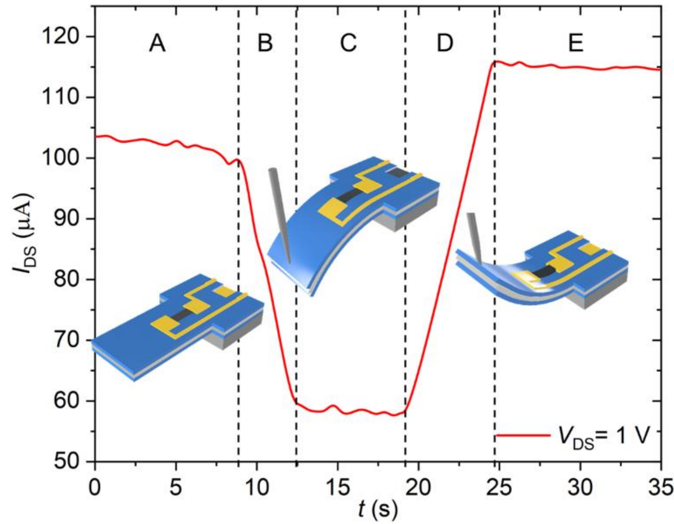

Figure 10. Time dependence of strain induction into graphene at constant V_{DS} = 1 V and V_{GS} = −3 V: region A) from ≈ 0 s to ≈ 8 s: cantilever in straight position with d_z = 0 μm; region B) from ≈ 8 s to ≈ 12 s: cantilever is bending down to d_z = −70 μm; region C) from ≈ 12 s to ≈ 19 s: cantilever bent at the position d_z = −70 μm; region D) from ≈ 19 s to ≈ 25 s: cantilever is bending up to +70 μm; region E) from ≈ 25 s to ≈ 35 s: cantilever bent at the position d_z = +70 μm.

For the second set of measurements, more precise control over the bend depth was introduced. We used probes which were placed on top at the free end of the cantilever in the perpendicular direction to its surface. These probes were controlled by a micromanipulator with ≈ 0.5 μm precision. We determined the distance per rotation of the microslider in the z-axis, enabling us to control the bending in the range of μm (Figure 11).

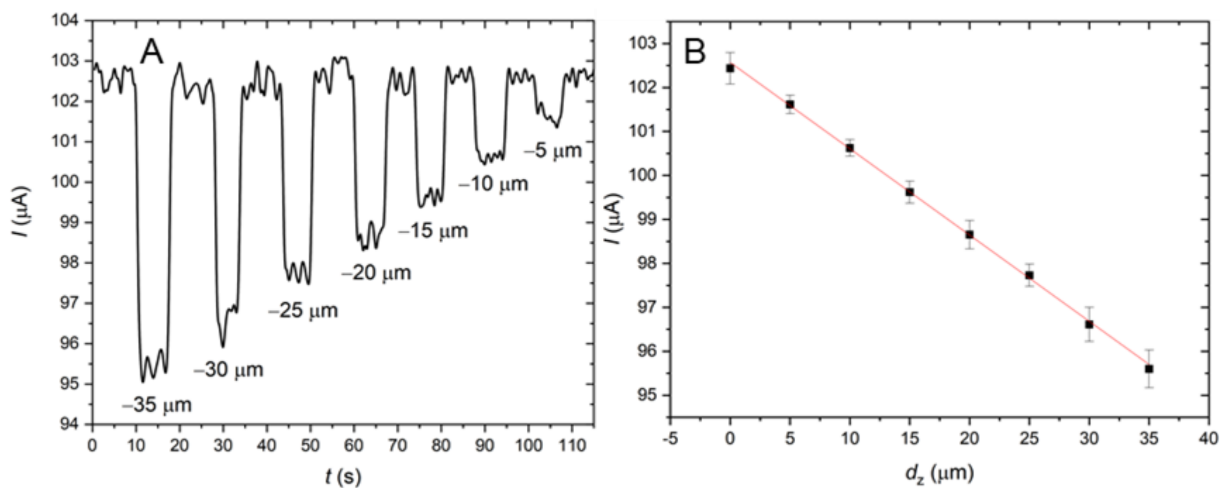

Figure 11. A) The decrease of I_{DS} for various bending depths; B) I_{DS} dependency on the bending, V_{GS} = 0 V, V_{DS} = 1 V

Position of the Dirac point voltage was determined in N_2 atmosphere, which ensured that no more undesired doping from air humidity took place. On one sample, the effect of Dirac point

voltage shift was observed after exposing the sample to air atmosphere, as shown in (Figure 12A).

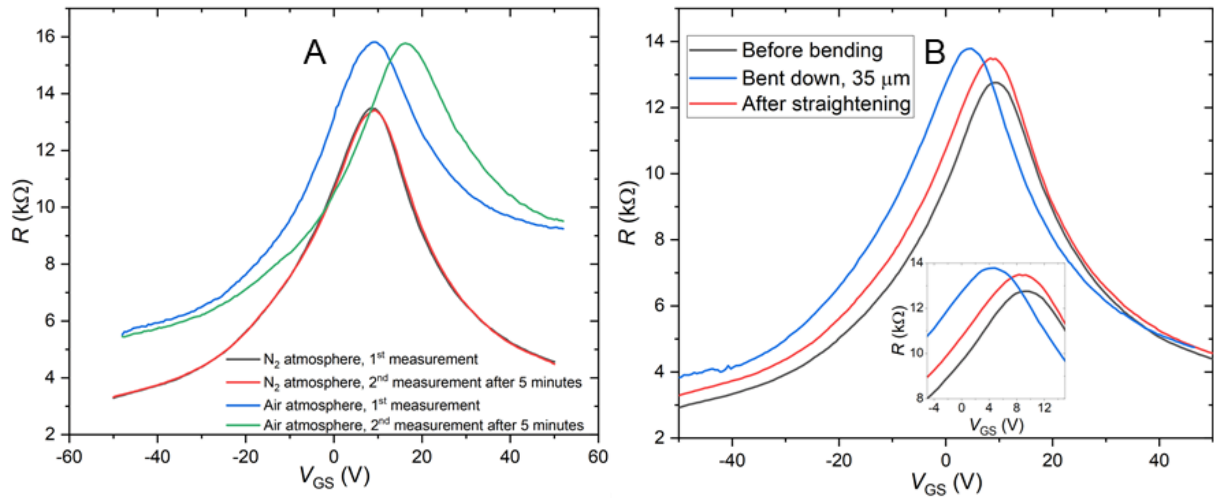

Figure 12. Transfer characteristics of graphene. A) Effect of atmosphere on Dirac point voltage; B) Shifting of the V_{Dirac} due to induced mechanical strain by bending

During the first measurement (Figure 12B) before bending of the cantilever, the V_{Dirac} of graphene was found at $V_{GS} \approx 9.3$ V. After bending of the cantilever in downwards direction, the shift of V_{Dirac} by ≈ 4.9 V was observed towards $V_{GS} \approx 4.4$ V, as captured in second sweep of the transfer characteristic. For the last sweep, the cantilever was returned to its original position. The V_{Dirac} was almost fully recovered to the same position as in the first measurement. The observed shift is a direct result of bending of the graphene sheet. The shift towards lesser values of V_{GS} means that the concentration of doped charge carriers (holes) is decreasing. Bending of the cantilever downwards induces tensile strain into the graphene, elongating the channel. This changes the distances between the atoms in crystal lattice and polarization occurs. The polarization creates electrical field in the channel. In order to compensate for the induced field, accumulation of electrons has to take place. These electrons recombine with holes; therefore, the concentration of holes decreases. This leads to the shift of V_{Dirac}. When the cantilever is bent upwards, the vector of polarization has the opposite direction. To compensate for the induced field, charge carriers of opposite polarity have to accumulate [32].

We observed that maximum tensile ε_{max} of ≈ 0.53% with corresponding σ_{max} of ≈ 2.59 GPa induced into graphene, caused a decrease of the I_{DS} by ≈ 10.9%. On the other side, the maximum ε_{max} of ≈ –0.41% with corresponding compressive σ_{max} of ≈ –2.58 GPa increased the I_{DS} by ≈ 4.1%. Our obtained results correspond well to results in other publications where the graphene was strained in uniaxial directions on other non-silicon substrates [33]. These obtained results of I_{DS} in combination with σ_{max} values predict the possibility of device fabrication with built-in stress. It is generally known that the values of residual stress, in order of GPa, are possible to fabricate. Additionally, there have been many papers describing the control of residual stress, well-suited for the fabrication of structures with built-in stress that bend after cantilever release. Such phenomena will cause induced strain in the graphene, and there will be no need to bend the cantilever manually by tip or any other method. The induced strain in graphene can be adjusted for the sensitivity and/or selectivity of sensor-based platforms [34]. Moreover, the work shows the magnitude of conductivity changes is in order of percent, which is comparable to a standard response of graphene FET-based gas and biosensors. Therefore, the induced strain artificially prepared, or as a result of a production process, must be considered.

4. Conclusions

We proposed and proved a new method for stretching of graphene 2DFET structure on a simple MEMS cantilever in Si technology. The bending of the cantilever with graphene was done using a micromanipulator with a micro-hook, which allowed us to bend the cantilever up and down along the z-axis but with moderate precision, nevertheless, it proved the functionality of structure. We achieved ε_{max} and σ_{max} values of ≈ 0.53% and ≈ 2.59 GPa, respectively, while the cantilever was bent down to –70 µm. When we bent the cantilever to the opposite side, up to +70 µm, we achieved an ε_{max} of ≈ –0.41% and an σ_{max} of ≈ –2.58 GPa, respectively. We next evaluated downward cantilever bending using a micromanipulator with a very thin and sharp tip with precision of ± 0.125 µm, which was placed on the cantilever end in the perpendicular direction. We were able to control the bending with d_z in the range from ≈ 0 µm to the ≈ −35

μm. Such stimuli had direct influence on resistivity and position of Dirac point. We observed significant changes in I_{DS} while the cantilever was bending; V_{GS} did not influence the perceptual change of I_{DS} because it only caused the shift along x-axis meaning the shift of Dirac point which is accompanied with change of physical properties mainly due to changes of atomic spacing causing the induction of local electric field. This results in the change of charge carrier concentration.

Our experiment proves the possibility of MEMS fabrication with controlled built-in residual stress, which will modulate the graphene's mechanical properties after the cantilever is released. Such a structure can be bent up or down according to the value of built-in stress, which can be comfortably controlled in order of GPa with utilization of standard physical vapor deposition methods, such as evaporation or sputtering. This work opens the door for sensitivity and selectivity selection by tuning the physical properties in graphene-based sensors, or alternatively, the same structures can be adapted to other 2DFET materials in silicon or eventually CMOS-based technology.

Acknowledgments

We acknowledge the support of the Grant Agency of the Czech Republic under contract GJ18-06498Y and CEITEC Nano Research Infrastructure (ID LM2015041, MEYS CR, 2016 2019), CEITEC Brno University of Technology. The infrastructure of the SIX Center of BUT was utilized to conduct the experiments. This work was also supported by the specific graduate research of the Brno University of Technology No. FEKT-S-20-6206.

References

1. Yang L, Xiao W, Wang J, Li X, Wang L (2021) Formaldehyde gas sensing properties of transition metal-doped graphene: a first-principles study. Journal of Materials Science 56 (21):12256-12269. doi:10.1007/s10853-021-05951-w
2. You X, Yang J, Dong S (2021) Structural and functional applications of 3D-printed graphene-based architectures. Journal of Materials Science 56 (15):9007-9046. doi:10.1007/s10853-021-05899-x
3. Schedin F, Geim AK, Morozov SV, Hill EW, Blake P, Katsnelson MI, Novoselov KS (2007) Detection of individual gas molecules adsorbed on graphene. Nature Materials 6 (9):652-655. doi:10.1038/nmat1967
4. Ohno Y, Maehashi K, Matsumoto K (2010) Chemical and biological sensing applications based on graphene field-effect transistors. Biosens Bioelectron 26 (4):1727-1730. doi:10.1016/j.bios.2010.08.001

5. Arash B, Wang Q, Duan WH (2011) Detection of gas atoms via vibration of graphenes. Phys Lett A 375 (24):2411-2415. doi:10.1016/j.physleta.2011.05.009
6. Yao Y, Chen XD, Guo HH, Wu ZQ (2011) Graphene oxide thin film coated quartz crystal microbalance for humidity detection. Appl Surf Sci 257 (17):7778-7782. doi:10.1016/j.apsusc.2011.04.028
7. Basu S, Bhattacharyya P (2012) Recent developments on graphene and graphene oxide based solid state gas sensors. Sensor Actuat B-Chem 173 (x):1-21. doi:10.1016/j.snb.2012.07.092
8. Qian Z, Hui Y, Liu F, Kang S, Kar S, Rinaldi M (2016) Graphene–aluminum nitride NEMS resonant infrared detector. Microsystems & Nanoengineering 2 (x):16026
9. Yi J, Lee JM, Il Park W (2011) Vertically aligned ZnO nanorods and graphene hybrid architectures for high-sensitive flexible gas sensors. Sensor Actuat B-Chem 155 (1):264-269. doi:10.1016/j.snb.2010.12.033
10. Wallace PR (1947) The Band Theory of Graphite. Phys Rev 71 (9):622-634. doi:DOI 10.1103/PhysRev.71.622
11. Novoselov KS, Geim AK, Morozov SV, Jiang D, Zhang Y, Dubonos SV, Grigorieva IV, Firsov AA (2004) Electric field effect in atomically thin carbon films. Science 306 (5696):666-669. doi:10.1126/science.1102896
12. Allen MJ, Tung VC, Kaner RB (2010) Honeycomb Carbon: A Review of Graphene. Chem Rev 110 (1):132-145. doi:10.1021/cr900070d
13. Fiori G, Bonaccorso F, Iannaccone G, Palacios T, Neumaier D, Seabaugh A, Banerjee SK, Colombo L (2014) Electronics based on two-dimensional materials. Nat Nano 9 (10):768-779. doi:10.1038/nnano.2014.207
14. Novoselov KS, Falko VI, Colombo L, Gellert PR, Schwab MG, Kim K (2012) A roadmap for graphene. Nature 490 (7419):192-200
15. Zhang ZH, Liu XF, Yu J, Hang Y, Li Y, Guo YF, Xu Y, Sun X, Zhou JX, Guo WL (2016) Tunable electronic and magnetic properties of two-dimensional materials and their one-dimensional derivatives. Wires Comput Mol Sci 6 (4):324-350. doi:10.1002/wcms.1251
16. Zhang XY, Xu ZW, Hui L, Xin J, Ding F (2012) How the Orientation of Graphene Is Determined during Chemical Vapor Deposition Growth. J Phys Chem Lett 3 (19):2822-2827. doi:10.1021/jz301029g
17. Biro LP, Nemes-Incze P, Lambin P (2012) Graphene: nanoscale processing and recent applications. Nanoscale 4 (6):1824-1839. doi:10.1039/c1nr11067e
18. Roldan R, Castellanos-Gomez A, Cappelluti E, Guinea F (2015) Strain engineering in semiconducting two-dimensional crystals. J Phys-Condens Mat 27 (31). doi:10.1088/0953-8984/27/31/313201
19. Yoon D, Son YW, Cheong H (2011) Negative Thermal Expansion Coefficient of Graphene Measured by Raman Spectroscopy. Nano Lett 11 (8):3227-3231. doi:10.1021/nl201488g
20. Lee C, Wei X, Kysar JW, Hone J (2008) Measurement of the Elastic Properties and Intrinsic Strength of Monolayer Graphene. Science 321 (5887):385
21. Lindahl N, Midtvedt D, Svensson J, Nerushev OA, Lindvall N, Isacsson A, Campbell EEB (2012) Determination of the Bending Rigidity of Graphene via Electrostatic Actuation of Buckled Membranes. Nano Lett 12 (7):3526-3531. doi:10.1021/nl301080v
22. Ding F, Ji HX, Chen YH, Herklotz A, Dorr K, Mei YF, Rastelli A, Schmidt OG (2010) Stretchable Graphene: A Close Look at Fundamental Parameters through Biaxial Straining. Nano Lett 10 (9):3453-3458. doi:10.1021/nl101533x
23. Si C, Sun ZM, Liu F (2016) Strain engineering of graphene: a review. Nanoscale 8 (6):3207-3217. doi:10.1039/c5nr07755a

24. Fischer AC, Forsberg F, Lapisa M, Bleiker SJ, Stemme G, Roxhed N, Niklaus F (2015) Integrating MEMS and ICs. Microsystems & Nanoengineering 1 (1):15005. doi:10.1038/micronano.2015.5
25. Hasan MM, Hossain MM (2021) Nanomaterials-patterned flexible electrodes for wearable health monitoring: a review. Journal of Materials Science 56 (27):14900-14942. doi:10.1007/s10853-021-06248-8
26. Grayson ACR, Shawgo RS, Johnson AM, Flynn NT, Li YW, Cima MJ, Langer R (2004) A BioMEMS review: MEMS technology for physiologically integrated devices. Proc IEEE 92 (x):6-21. doi:10.1109/jproc.2003.820534
27. Mathew R, Ravi Sankar A (2018) A Review on Surface Stress-Based Miniaturized Piezoresistive SU-8 Polymeric Cantilever Sensors. Nano-Micro Letters 10 (2):35. doi:10.1007/s40820-018-0189-1
28. Gayathri S, Jayabal P, Kottaisamy M, Ramakrishnan V (2014) Synthesis of few layer graphene by direct exfoliation of graphite and a Raman spectroscopic study. AIP Advances 4 (2):027116. doi:10.1063/1.4866595
29. Wu J-B, Lin M-L, Cong X, Liu H-N, Tan P-H (2018) Raman spectroscopy of graphene-based materials and its applications in related devices. Chemical Society Reviews 47 (5):1822-1873. doi:10.1039/C6CS00915H
30. Melios C, Giusca CE, Panchal V, Kazakova O (2018) Water on graphene: review of recent progress. 2D Materials 5 (2):022001. doi:10.1088/2053-1583/aa9ea9
31. Bartošík M, Mach J, Piastek J, Nezval D, Konečný M, Švarc V, Ensslin K, Šikola T (2020) Mechanism and Suppression of Physisorbed-Water-Caused Hysteresis in Graphene FET Sensors. ACS Sensors 5 (9):2940-2949. doi:10.1021/acssensors.0c01441
32. Hu G, Wu J, Ma C, Liang Z, Liu W, Liu M, Wu JZ, Jia C-L (2019) Controlling the Dirac point voltage of graphene by mechanically bending the ferroelectric gate of a graphene field effect transistor. Materials Horizons 6 (2):302-310. doi:10.1039/C8MH01499J
33. Topsakal M, Bagci K, Ciraci S (2010) Current-voltage (I-V) characteristics of armchair graphene nanoribbons under uniaxial strain. Physical Review B 81 (x). doi:10.1103/PhysRevB.81.205437
34. Cao ZX, Yao BC, Qin CY, Yang R, Guo YH, Zhang YF, Wu Y, Bi L, Chen YF, Xie ZD, Peng GD, Huang SW, Wong CW, Rao YJ (2019) Biochemical sensing in graphene-enhanced microfiber resonators with individual molecule sensitivity and selectivity. Light-Sci Appl 8 (107). doi:10.1038/s41377-019-0213-3